Field and satellite observations of the formation and distribution of Arctic atmospheric bromine above a rejuvenated sea ice cover

Son V. Nghiem[1], Ignatius G. Rigor[2], Andreas Richter[3], John P. Burrows[3,4], Paul B. Shepson[5], Jan Bottenheim[6], David G. Barber[7], Alexandra Steffen[6], Jeff Latonas[7], Feiyue Wang[7,8], Gary Stern[7,9], Pablo Clemente-Colón[10], Seelye Martin[11], Dorothy K. Hall[12], Lars Kaleschke[13], Philip Tackett[5], Gregory Neumann[1], and Matthew G. Asplin[7]

[1]Jet Propulsion Laboratory, California Institute of Technology, Pasadena, CA, USA
Son.V.Nghiem@jpl.nasa.gov

[2]Polar Science Center, Applied Physics Laboratory, University of Washington, Seattle, WA, USA

[3]Institute of Environmental Physics, University of Bremen, Bremen, Germany

[4]Biogeochemistry Programme, NERC Centre for Ecology and Hydrology, Wallingtonford, Oxfordshire, UK

[5]Purdue Climate Change Research Center, Departments of Chemistry and Earth and Atmospheric Sciences, Lafayette, IN, USA

[6]Science and Technology Branch, Environment Canada, Toronto, ON, Canada

[7]Center for Earth Observation Science, Faculty of Environment, Earth and Resources, University of Manitoba, Winnipeg, MB, Canada

[8]Department of Chemistry, University of Manitoba, Winnipeg, MB, Canada

[9]Freshwater Institute, Department of Fishery and Oceans, Winnipeg, MB, Canada

[10]National Ice Center, Washington, DC, USA

[11]School of Oceanography, University of Washington, Seattle, WA, USA

[12]NASA Goddard Space Flight Center, Greenbelt, MD, USA

[13]Institute of Oceanography, University of Hamburg, Hamburg, Germany

Abstract

Recent drastic reduction of the older perennial sea ice in the Arctic Ocean has resulted in a vast expansion of younger and saltier seasonal sea ice. This increase in the salinity of the overall ice cover could impact tropospheric chemical processes. Springtime perennial ice extent in 2008 and 2009 broke the half-century record minimum in 2007 by about one million km^2. In both years seasonal ice was dominant across the Beaufort Sea extending to the Amundsen Gulf, where significant field and satellite observations of sea ice, temperature, and atmospheric chemicals have been made. Measurements at the site of the Canadian Coast Guard Ship Amundsen ice breaker in the Amundsen Gulf showed events of increased bromine monoxide (BrO), coupled with decreases of ozone (O_3) and gaseous elemental mercury (GEM), during cold periods in March 2008. The timing of the main event of BrO, O_3, and GEM changes was found to be consistent with BrO observed by satellites over an extensive area around the site. Furthermore, satellite sensors detected a doubling of atmospheric BrO in a vortex associated with a spiral rising air pattern. In spring 2009, excessive and widespread bromine explosions occurred in the same region while the regional air temperature was low and the extent of perennial ice was significantly reduced compared to the case in 2008. Using satellite observations together with a Rising-Air-Parcel model, we discover a topographic control on BrO distribution such that the Alaskan North Slope and the Canadian Shield region were exposed to elevated BrO, whereas the surrounding mountains isolated the Alaskan interior from bromine intrusion.

1. Introduction

Arctic sea ice in late summer or early fall has recently undergone a drastic reduction in its total extent, far exceeding the worst-case projections by climate models reported in the Intergovernmental Panel on Climate Change Fourth Assessment Report [*Stroeve et al*, 2007; *Allison et al*., 2009]. More important than the minimum total sea ice extent in summer, the changing composition of Arctic sea ice classes in late winter and spring plays a major role in tropospheric photochemical processes during polar sunrise at higher latitudes [*Simpson et al*., 2007b]. This study addresses changes in tropospheric chemistry as well as the oxidizing capacity of the lower troposphere and related environmental impacts associated with the observed changing sea ice composition.

As a result of the large loss of perennial sea ice, the overall composition of springtime Arctic sea ice cover has changed in recent years, becoming dominated by younger and thinner seasonal sea ice [*Nghiem et al*., 2007]. The latter consists of sea ice with a more briny surface, together with more refrozen leads, polynyas, and frost flowers. The salinity and surface conditions of these sea ice types may affect the release of molecular bromine and bromine chloride [*Foster et al*., 2001; *Huff and Abbatt*, 2002]. These molecules are easily photolyzed by sunlight leading to the production of atomic bromine and chlorine, which participates in a catalytic cycle removing ozone (O_3) [*Barrie et al*., 1988; *Fan and Jacob*, 1992, *Foster et al*., 2001, *Simpson et al*., 2007b] and gaseous element mercury (GEM) [*Schroeder et al*., 1998, *Steffen et al*., 2008]. Because mercury is toxic, deposition of GEM oxidation products can have significant impacts on the Arctic biosphere and its biogeochemistry [*Fishman*, 1991; *Lu et al*., 2001; *Steffen et al*., 2008, *Stephens et al*., 2011]. GEM depletion may enhance Arctic mercury deposition affecting the health of people and wildlife [*AMAP/UNEP*, 2008]. Increasing scientific knowledge of mercury

processes is important to the intergovernmental negotiation for global action on mercury to protect human health and the environment [*UNEP*, 2011].

With measurements from multiple, coordinated research projects during the International Polar Year (IPY), including the Circumpolar Flaw Lead (CFL) System Study, the Ocean Atmosphere Sea Ice Snowpack (OASIS) campaign, and the State of Arctic Sea Ice Cover project, the present study employs a unique combination of surface based and satellite borne measurements to examine the Arctic sea ice change and its impacts on photochemical processes across the Alaskan and the adjacent Canadian Arctic sea ice sector during the polar sunrise periods in 2008 and in 2009. Summarized with the chart in Figure 1, this effort aims, in the spirit of IPY, to examine in an integrated manner the relationships between photochemical processes, transport, and distribution in a changing Arctic, especially in view of the drastic reduction of perennial sea ice that has resulted in a predominance of the younger and saltier seasonal sea ice in the last decade. Chemical measurements of bromine, ozone, and mercury data were obtained from field campaigns and from satellite sensors for both surface and vertical column observations. To investigate chemical sources and subsequent processes, necessary environmental data characterizing sea ice, snow, frost flowers, leads, and their dynamic and thermodynamic change and distribution were collected with field measurements and multiple satellite observations. Atmospheric data, including horizontal wind field and vertical motion (omega field characterizing ascending and descending air masses) under variable conditions of atmospheric pressure and temperature, were used to examine the chemical transport and distribution.

2. Arctic Conditions during the Spring Transition in 2008

While the 2007 record minimum of total sea ice extent in summer has been widely reported [*Maslanik et al*., 2007; *Perovich et al*., 2008; *Richter-Menge et al*., 2008], the impact of sea ice composition in terms of partitioning between perennial and seasonal ice within the total ice extent in springtime, relevant to photochemically induced catalytic processes, involving BrO, O_3, and GEM, has not been considered previously. In March, the perennial ice extent in 2008 shattered the 50-year record set in 2007 by one million km^2, i.e. about half of the surface area of Greenland, as observed from a comparison of the perennial ice extent in 2008 (Figure 2) and in 2007 and earlier years [*Nghiem et al*., 2007].

Figure 2a presents the synoptic state of Arctic sea ice on 15 March 2008. This is a new composite product for sea ice mapping, which utilizes the capability of QuikSCAT (QS) scatterometer data for automatic ice identification on large scales, together with high-resolution features identified from synthetic aperture radar (SAR) data acquired by the European Space Agency's Envisat Advanced SAR (ASAR). The sea ice cover is dominated by seasonal ice having an extent of 8.9 ± 0.2 million km^2, about 3.4 times the extent of perennial ice (excluding mixed ice). The boundary of seasonal ice in Figure 2 had already migrated across the North Pole towards Canada before the end of February 2008 due to wind forcing for the first time as observed in the history of sea ice charting at the U.S. National Ice Center, which began in the 1970s. In the sector from the Beaufort Sea to the Amundsen Gulf (BSAG), seasonal ice occupied a vast expanse from the coastline northward.

Seasonal sea ice is much more saline than perennial ice, which is desalinated by gravity drainage of the surface melt water during summer [*Weeks and Ackley*, 1982]. The salinity depth profile in seasonal ice has a characteristic C shape with higher salinity near the snow-ice and the

ice-water interfaces and lower salinity in the internal section [*Weeks and Ackley*, 1982]. In the basal snow layer overlying the sea ice interface, the salinity is characteristically high, as much as 10 psu or higher, as a result of brine wicked up from the underlying sea ice through brine channels. However, the salinity rapidly decreases toward the snow surface as more fresh snow accumulates. This is the typical salinity profile of the snow cover on Arctic sea ice with the upper fresh snow burying the basal saline snow adjacent to the sea ice interface [*Barber et al.*, 1995].

In-situ measurements from a field campaign, which took place in March 2008 as part of the International Polar Year (IPY) Circumpolar Flaw Lead (CFL) System Study [*Barber et al.*, 2010], showed that salinity was in the range of 1-20 psu in 1-5 cm of the basal snow, which was buried under 5-40 cm of mostly fresh snow (0-1 psu, with 0 psu in the top layer in most cases) on the sea ice in the Amundsen Gulf [*Chaulk et al*., 2011]. This observation is in agreement with previous measurements showing that the high salinity is confined to the basal layer underneath the fresh snow in the upper layer, e.g., from the Seasonal Sea Ice Monitoring and Modelling field campaign [*Barber and Nghiem*, 1999] and from a field investigation of bromoform ($CHBr_3$) in the Arctic atmospheric bromine budget [*Sturges et al*., 1997].

Sea ice deformation was particularly strong in the winter and spring of 2008. The sea ice cover was ravaged and broken into small floes, even in perennial ice areas seen as a composition of fragmented pieces (see inside the white circle in Figure 2a). Daily QS sea ice maps for February-March 2008 indicate that the perennial ice pack, which had abutted the west coast of Banks Island in early February, was detached and diverted westward. This ice divergence created numerous open water areas (leads, polynyas) in BSAG where new thin ice and frost flowers formed highly saline surfaces.

Figure 2b, a high-resolution RADARSAT SAR image from 16 March 2008, shows that many leads are elongated. In an ice divergence area, because frost flowers are associated with strong radar backscatter [*Nghiem et al*., 1997a], bright features in leads, such as the bright elongated feature in the ellipse in Figure 2b, indicate the presence of frost flowers. A lead without frost flowers would have low backscatter [*Nghiem et al*., 1995]. Figure 2c shows an example of needle-shaped frost flowers observed in a lead in the Amundsen Gulf during the IPY CFL field campaign in March 2008. The needle-shape indicates that they formed under very cold conditions [*Martin et al*., 1995, 1996; *Perovich and Richter-Menge*, 1994], such as those associated with the rapid growth of new sea ice in leads. The sea ice growth rate doubles when air temperature decreases from –18^{o}C to –30^{o}C [*Wakatsuchi and Ono*, 1983; *Nghiem et al*., 1997b]. At colder air temperatures, frost flowers have a higher salinity [*Martin et al*., 1996]. In summary, thin saline sea ice rapidly forms in leads and establishes a substrate upon which frost flowers grow, wick up brine, and further increase the surface salinity. CFL field measurements in early and late March 2008 showed that frost flower salinities were in the range of 110-140 psu, or about four times the salinity of the underlying Arctic seawater.

In March 2008, the BSAG sector was often colder than average for this month. Surface air temperature (SAT) data from the National Centers for Environment Prediction **(**NCEP) [*Kalnay et al*., 1996] show a negative anomaly of about 4^{o}C in March 2008, below the 1948-2008 average. Satellite ice surface temperature (IST) derived from the NASA Moderate Resolution Imaging Spectroradiometer (MODIS) [*Hall et al*., 2004] was particularly low in the CFL area (Figure 2) during 12-19 March 2008. Daily IST, averaged over the area within 69-74^{o}N and 120-150^{o}W in BSAG, ranged from –29.2^{o}C to –19.2^{o}C with the lowest value observed on 17th March (top panel in Figure 3). These low temperatures are consistent with buoy data (top panel

in Figure 3) from the International Arctic Buoy Programme [*Rigor et al*., 2000], including Buoy 66276 (72.9^{o}N, 128.9^{o}W, west of Banks Island) and Buoy 05314 (73^{o}N, 144.2^{o}W, farther west in the Beaufort Sea). These low temperatures would induce the formation of a saltier ice surface and conditions, including a stable boundary layer, conducive to triggering a bromine explosion [*Wennberg*, 1999; *Tarasick and Bottenheim*, 2002; *Kaleschke et al*., 2004; *Sander et al*., 2006].

3. Potential Sources for BrO Enhancement and O_3 and GEM Depletions

The oceanic biosphere releases a variety of organic halogen-containing species, which enter the planetary boundary layer and eventually release halogens. However, these organohalogens are not rapidly photolyzed by natural sunlight, react slowly and sufficiently with oxidizing agents such as OH, and hence are not believed to play a major role in the production of molecular halogen species such as molecular bromine and bromochlorine. Rather, the inorganic acid-catalysed equilibria between halides and hypohalites in the surface ice result in the formation of molecular halogens and interhalogens, which are then emitted [*Huff and Abbatt*, 2002; *Abbatt et al*., 2010]. These reactions have been identified as a strong source of atmospheric bromine at high latitudes. Although much progress has been made, the details of the physical-chemical mechanism releasing bromine from sea salt to the gas phase remain controversial [*Simpson et al*., 2007a]. Here, we discuss several potential bromine sources given the snow and sea ice observations presented in the above section.

The reactions on the cold saline surfaces of frost flowers and/or the resulting cold saline aerosol have been proposed as playing a key role in triggering and releasing bromine [*Hall and Wolff*, 1998; *Rankin et al*., 2002; *Kaleschke et al*., 2004; *Jacobi et al*., 2006; *Sander et al*., 2006; *Simpson et al*., 2007a]. It is known that these reactions are acid catalyzed [*Huff and Abbatt*, 2002], a condition that is fulfilled at low temperature by precipitation of carbonates and other

salts, hence reducing buffering [*Sander et al*., 2006; *Sander and Morin*, 2009; *Dieckman et al*., 2010].

Frost flowers were observed in BSAG during the CFL field campaign (Figure 2). Along the ship track of the TARA [*DAMOCLES*, 2009], Bottenheim et al. [2009] observed tropospheric ozone depletion episodes (ODEs) at large distances downwind from the Siberian coast where large flaw leads and gigantic polynyas formed, having extensive frost-flower cover in the spring of 2007. However, direct evidence of bromine release is sparse due to difficulties in making chemical observations near frost flowers [*Simpson et al*., 2007a]. Frost flowers are hypothesized to be an indirect source of reactive bromine by producing cold highly saline aerosols.

The presence of BrO at high altitudes would require recycling on lofted aerosol [*Kaleschke et al*., 2004; *Sander et al*., 2006; *Simpson et al*., 2007a; *Begoin et al*., 2010], which could also enhance bromine by scavenging hydrogen bromide (HBr). Given the large seasonal sea ice extent in BSAG, many leads were created by the ice dynamics (Figure 2). A possible lofting mechanism is the buoyant convection that forms plumes emanating from leads [*Glendening*, 1995; *Alam and Curry*, 1995; *Pinto and Curry*, 1995; *Pinto et al*., 1995; *Burk et al*., 1997; *McElroy et al*., 1999; *Zulauf and Krueger*, 2003]. Observations of convective plumes over leads indicate that lead-generated clouds can penetrate a wintertime inversion of up to 4 km in height and persist for 250 km downwind [*Schnell et al*., 1989]. High concentrations of mercury have been observed near Arctic leads that had convective plumes [*Douglas et al*., 2005], indicating potential mercury deposition from mercury depletion events (MDEs). Current atmospheric chemical models have not fully incorporated plumes and thus miss these effects.

The snow cover over the large extent of seasonal sea ice in BSAG (Figure 2) can be a potentially important factor impacting bromine processes. Based on a higher correlation of BrO

with seasonal ice contact compared to that of potential frost flower contact, Simpson *et al.* [2007b] note that snow contaminated with sea salts on first-year sea ice is a more probable bromine source than are frost flowers. However, there is a large uncertainty in such analysis because of the use of satellite passive microwave data, which suffer from land contamination especially in coastal regions and have limited capability due to their low spatial resolution.

Using mean snow salinity in a model developed for Antarctic conditions, *Yang et al*. [2008] suggested snow cover on sea ice could be a potential source of bromine release, with aerosol production from blowing snow being more than an order of magnitude greater than that from the open ocean. However, unlike the salinity distribution in snow due to heavy snow loading and flooding on Antarctic sea ice, the salinity in Arctic snow mainly resides in the basal snow layer while the upper snow cover primarily consists of freshwater snow, as was also observed by snow measurements during CFL. If a mean value of snow salinity is used in lieu of a salinity profile, the modeled distribution of salinity is in effect constant throughout the snow layer. This is not representative of the typical snow salinity profile on Arctic sea ice, and it artificially redistributes a significant amount of salinity from the basal snow to the top snow cover surface.

Sea spray can be a mechanism that deposits sea salt on snow-covered sea ice. In the Laptev Sea to the east of the Taymyr Peninsula in spring 2007, strong winds created a giant polynya as large in area as Austria. This extensive polynya endured a rough sea state with gale-force winds (17-20 m/s in the Beaufort scale) that may have transported sea salt to the snow-covered surface of sea ice [*Bottenheim et al*., 2009]. Similar strong winds over large leads produce sea sprays and distribute sea salt to the adjacent sea ice, or in the case of coastal leads, to land. However, this mechanism requires both high winds and a large expanse of open water for the development of a high sea state, and such conditions were not observed over BSAG.

While the precise origins of bromine sources remain unresolved and require further investigation, a common denominator is that a saltier environment resulting in cold brine should lead to more bromine explosions. In this regard, the increased prevalence of salty seasonal sea ice across the Arctic enhances the potential sources of cold brine and thus facilitates the process of extensive bromine release.

4. Photochemical Processes

As outlined above, the photochemically labile species, Br_2 and BrCl are released through complex multiphase reactions. In springtime, gaseous Br_2 is rapidly photo-dissociated into Br atoms, which participate in cycles catalytically destroying O_3 and oxidizing GEM with the Br atoms being regenerated in excess in this autocatalytic process. HOBr produced in a termination step deposits to saline surfaces, generating Br_2 which evolves to the gas phase, in the process providing twice as many Br atoms back to the gas phase, and hence the term "bromine explosion" evoleved to describe this behavior [*Wennberg*, 1999]. Details of these chemical processes can be found in the literature [e.g., *Fan and Jacob*, 1992; *Kaleschke et al*., 2004; *Sander et al*.; 2006, ; *Simpson et al*., 2007a; *Piot and von Glasow*, 2008], and the two most important cycles, which require sunlight (*hv*), are summarized as follows:

Cycle 1:

$$Br_2 + h\nu \rightarrow Br + Br \quad (1)$$

$$2(Br + O_3 \rightarrow BrO + O_2) \quad (2)$$

$$2[BrO + HO_2 \rightarrow HOBr(g) + O_2] \quad (3)$$

$$2[HOBr(g) \rightarrow HOBr(l)] \quad (4)$$

$$2[HOBr(l) + HBr(l) \rightarrow H_2O(l) + Br_2(g)] \quad (5)$$

Net: $2HO_2 + 2HBr + 2O_3 + h\nu \rightarrow 2H_2O + Br_2 + 4O_2$

Cycle 2:

$BrCl + h\nu \rightarrow Cl + Br$ (6)

$Br + O_3 \rightarrow BrO + O_2$ (2)

$Cl + O_3 \rightarrow ClO + O_2$ (7)

$BrO + HO_2 \rightarrow HOBr(g) + O_2$ (3)

$ClO + HO_2 \rightarrow HOCl(g) + O_2$ (8)

$HOBr(g) \rightarrow HOBr(l)$ (4)

$HOBr(l) + HCl(l) \rightarrow H_2O(l) + BrCl(g)$ (9)

Net: $2HO_2 + HCl(l) + 2O_3 + h\nu \rightarrow H_2O + HOCl(g) + 4O_2$

Note that the effective equilibria (5) and (9) are complex themselves:

$H^+ + Cl^- + HOBr(l) \rightarrow H_2O + BrCl(l)$

$BrCl(l) \rightarrow BrCl(g)$

$BrCl + Br^- \rightarrow Br_2Cl^-$ (10)

$Br_2Cl^- \rightarrow Br_2 + Cl^-$

Net: $H^+ + Br^-/Cl^- + HOBr \rightarrow H_2O + Br_2/BrCl$

Both cycles (1) and (2) require a source of H atoms such as the free radical HO_2. Cycle 1 destroys O_3 and is autocatalytic in that it releases one additional Br atom to the gas phase per cycle. This increases the concentration of the chain carrier Br atoms and as a result, also increases the rate of removal of O_3 by reaction (2). Cycle 2 also destroys O_3 but the rate of O_3

destruction is dependent on the concentration of the chain carriers Cl-atoms and Br atoms. The former unlike the latter react in the atmosphere with CH_4, thus terminating the chain reaction. The chain length for cycle (2) is therefore likely to be shorter than that for Cycle 1. Cycle 1 and Cycle 2 can be named bromine explosion and Br-catalyzed chloride oxidation reations.

The liquid phase reactions (5) and (9) consume acidity. Sander et al. [2006] proposed that the triggering of these reactions could result from the change of ionic concentration in the brine by the precipitation of ikaite ($CaCO_3 \cdot 6H_2O$) at –2.2 °C, mirabilite ($Na_2SO_4 \cdot 10H_2O$) at –8.2°C and hydrohalite ($NaCl \cdot 2H_2O$), by the acid-catalyzed equilibria, and by the temperature dependences of the equilibrium reactions in the above scheme. Dieckmann et al. [2010] reported observations of calcium carbonate crystals in Arctic sea ice and the polymorphic form of ikaite. Rysgaard et al. [2011] indicate that the ikaite component of the calcium carbonate cycle may also be important in overall air-surface CO_2 fluxes.

Correlated with O_3 depletion, GEM depletion also occurs in a similar rapid process involving bromine [*Lu et al*., 2001; *Gauchard et al*., 2005; *Steffen et al*., 2008]. Consequently, elemental mercury (Hg^0) is oxidized to Hg^{II} (or Hg^{I}) in the atmosphere, and this more reactive inorganic Hg species can then be deposited into the ocean and on the land surface. While a fraction of the deposited Hg^{II} is reduced through photo reduction processes and re-emitted as GEM back into the atmosphere [*Lalonde et al*., 2003; *Steffen et al*., 2008; *Sherman et al*., 2011] some of this deposited $Hg^{I \text{ or } II}$ can remain on/in the deposited surface [*Durnford et al*., 2011]. The salinity of the Arctic Ocean surface may play a role in suppressing the reduction and re-emission of the deposited Hg [*St. Louis et al*., 2005]. There are significant uncertainties in the mass balance of mercury between air, surface and the ocean [*Outridge et al*., 2008], suggesting not all the processes occurring in the Arctic are currently understood [*Steffen et al*., 2008].

5. Field Measurements and Satellite Observations

While the importance of bromine photochemistry in the depletion of polar ozone and GEM is established, knowledge of the physical link between Arctic sea ice reduction and the distribution, spatial extent, and time scale of bromine activation is limited. In this regard, during the 2008 IPY CFL and the Ocean Atmosphere Sea Ice Snowpack [*Shepson et al*., 2003] - Canada (OASIS-CANADA) campaigns at the site of the Canadian Coast Guard Ship (CCGS) Amundsen, measurements of BrO, O_3, and GEM were made. BrO data were collected at 71.07^{o}N and 123.46^{o}W. Ozone was monitored with an ozone sensor based on ultraviolet absorption measurements (TEI model 049). GEM was measured by cold vapor atomic fluorescence spectroscopy [*Steffen et al*., 2008].

In the Amundsen Gulf, BrO and O_3 (OASIS) and GEM (CFL) showed several transient episodes of bromine increase, concurrent with depletions of ozone and mercury (Figure 3). GEM is considered depleted from the atmosphere when it falls below ~1 ngm^{-3} [*Cole and Steffen*, 2010]. The black arrows in Figure 3 mark notable episodes. These occurred during cold periods, as indicated by cold air temperatures measured by buoys in the BSAG region of the experiment, in agreement with the observations of Tarasick and Bottenheim [2002] and the mechanism proposed by Sander et al. [2006]. NCEP data show that cold air was advected into BSAG by the northerly component of the surface wind persistent in March 2008. Before 13 March, average wind speeds were low to medium (< 7 m s^{-1}), which supported stable boundary layer conditions conducive to a bromine explosion.

While the OASIS and CFL chemical measurements were made at specific locations near the surface, the Global Ozone Monitoring Experiment-2 (GOME-2) and Scanning Imaging Absorption Spectrometer for Atmospheric Cartography (SCIAMACHY) satellite data were used

to retrieve the integrated atmospheric vertical column (VC) of BrO at their respective spatial resolutions using Differential Optical Absorption Spectroscopy [*Sinnhuber et al*., 2005; *Richter et al*., 1998; *Begoin et al*., 2010]. Data from SCIAMACHY and GOME-2 were cross-calibrated. Details of SCIAMACHY and GOME-2 data processing were presented in the relevant Algorithm Theoretical Basis Documents (*DLR*, 2009; *DLR*, 2011). For comparison with the ground-based measurements, the VC BrO was collated within a 200 km radius around the CFL location and spatially averaged for each day in March 2008.

Values of VC BrO from GOME-2 were slightly lower than those from SCIAMACHY, which had a slightly higher spatial resolution and made measurements about 30 minutes after those of GOME-2. For the period from 12-19 March 2008, both datasets identified significantly elevated BrO (Figure 3). In this same period, persistent ozone and mercury depletions were observed at the CFL field location as indicated by the observed low values of OASIS O_3 and GEM, while the ice surface was very cold, i.e., –28^{o}C (average IST from the MODIS sea ice data product). A comparison of BrO measurements by OASIS ground-based long-path differential optical absorption spectroscopy (LP-DOAS) with GOME-2 data indicated a good agreement, when the elevated VC BrO was assumed to be located within the atmospheric boundary layer [*Pöhler et al*., 2010].

The peak value of VC BrO on 14 March 2008, within the period marked by the orange double-arrow line in Figure 3, was about double the value before the BrO enhancement period. These high values of VC BrO continued through 15 March, though being slightly lower than that on 14 March, in agreement with the LP-DOAS surface observations when the BrO enhancement is restricted to the troposphere [*Pöhler et al., 2010*]. Surface winds became strong on 13 March and continued to be strong on 14 and 15 March, when it appeared that BrO continued to rise and

perhaps recycle in the atmosphere along long-range trajectories. However, the spread of bromine could also occur through a series of deposition and reemission of bromine, called leap-frogging, as the air drifted away from the bromine source, allowing the bromine to appear farther downwind [*Piot and von Glasow*, 2008]; this process exhibits stop-and-go behavior with the BrO production being modulated by the amount of actinic solar radiation.

VC BrO abruptly decreased on 16 March and continued decreasing in the following days. This abrupt decrease occurred when Figure 3 shows that the surface temperature was cold and the NCEP analysis indicated that upwelling winds still occurred over BSAG. These conditions should have maintained the high level of VC BrO over BSAG. Several explanations can be proposed for this abrupt BrO reduction. First, strong winds cause rapid vertical mixing and horizontal spreading, thereby diluting BrO at lower altitudes over a larger area. Since the rate of the chain propagation reaction is proportional to $[BrO]^2$, a BrO dilution will substantially slow the ozone depletion chemistry. In support of this explanation, we note that Seabrook et al. [2011] report on differential absorption LIDAR (DIAL) measurements of the vertical profile of ozone in the first km above the surface, showing an enhanced surface boundary layer depth on March 16. Second, lower surface radiation would also slow the photochemical processes. Third, strong winds may have forced extensive drifting of fresh snow that buried the highly saline frost flowers and slush layers and thus shut down the BrO source in the area. This shutting down by drifting snow of active bromine sources contrasts with the blowing snow mechanism across the Antarctic sea ice [*Jones et al*., 2010], which has been theoretically proposed to enhance the BrO [*Yang et al*., 2008]. The latter mechanism requires that a significant amount of sea salt lies on the snow surface or in the upper layers of the snow cover, which is not the case for the Arctic snow cover observed in this study.

Drifting fresh snow could diminish the bromine source in two ways:

(1) Snow grains could attach to frost flower crystals (see Figure 2c taken on 16 March) and could prevent the salt-laden crystals from becoming cold aerosols, and

(2) Snow could bury the highly saline frost flowers and saline slush patches on the sea ice surface, which could then hinder the sea salt release into the atmosphere. In this scenario, the strong winds initially uplift salty aerosols, but this process is then terminated by the fresh snow cover.

The field observations show three snow-drifting events on 16, 24, and 27 March, as indicated by the magenta arrows in Figure 3. On 17 March, VC BrO continued to decline, while the upwelling became stronger (up to 0.7 km compared to the typical 0.4 km). We infer from these observations that the bromine recycling process was running out of fuel after its initial source was shut down because the bromine recycling cannot be sustained without an effective supply of bromine. Following the first blowing snow event on 16 March, the events on 24 and 27 of March also coincided with a decrease in VC BrO and an increase in O_3 and GEM in both cases (Figure 3). The results also indicate VC BrO decreases farther away from the triggering source in space and in time as the transport and recycling processes wane [*Frieß et al*., 2004].

The better coverage of the GOME-2 instrument, compared to SCIAMACHY, enabled observations of the spatial distribution of VC BrO over BSAG. Figure 4 shows results for 13-18 March 2008 (days 73-78 in 2008). VC BrO enhancement was also detected over sections of BSAG on 12 and 19 March 2008 when the GOME-2 measurements had only partial coverage of BSAG and therefore are not included in the figure. On 13 March 2008, the VC BrO cloud was part of a well-defined vortex or spiral pattern with its center located near the northeast coast of Victoria Island. To the west of this vortex, VC BrO stretched westward along the northern

coastal region of Alaska. On the next day, the center of the vortex pattern shifted to the southeast coast of Victoria Island, while the VC BrO along the Alaskan coast strengthened. This is the first documented report of BrO forming into a pronounced and well-defined vortex. The importance of satellite spatial data in identifying synoptic BrO patterns is noted here: a Gedanken-experiment flight line into the BrO vortex may erroneously suggest the potential existence of sheets of BrO or pockets of BrO roaming the Arctic.

By 15 March 2008, Figure 4 shows that large values of VC BrO remained over the Amundsen Gulf, while the vortex became less pronounced and the VC BrO along the Alaskan North Slope weakened. From 13 to 16 March 2008, VC BrO was observed farther south in the Canadian Shield region (see this region on maps in the National Geographic Atlas of the World [*Allen*, 1995]) to the east of the Richardson and Mackenzie Mountains, while the Alaskan BrO was restricted to the north of the Alaskan Brooks Range. On 16 March 2008, VC BrO decreased in the Amundsen Gulf, while stretching extensively to the west in the Beaufort Sea and in the North Slope. For 17-18 March 2008, VC BrO decreased significantly in BSAG, while high VC BrO was still observed around Victoria Island extending into the Canadian Shield region. The decreasing trend corresponded to the waning phase of VC BrO (Figure 3). Despite the spatial-scale difference between satellite and surface measurements, both consistently observe the timing of the main event of the BrO enhancement and the associated O_3 and GEM depletions.

6. Dynamics and Distribution of BrO

To provide insights into the process of the dynamics and distribution of VC BrO observed by GOME-2, we have developed a Rising Air Parcel (RAP) model, which operates as follows: (1) Parcels of air are initiated from surface areas that are first-year and mixed sea ice, cold, and rising vertically as defined by the NCEP omega wind fields; (2) the parcels are then traced over a

one-week period through the three-dimensional wind fields; and (3) the parcel traces are terminated if the parcels intersect topography. Given the salinity differences between perennial and first-year ice described in Section 2, QS daily maps of sea ice classes [*Nghiem et al*., 2007] were used to include air parcels rising from sea ice that is not perennial ice. We use the NCEP wind and temperature fields to derive the patterns of rising air parcels shown in Figure 5, where information on the partition of different sea ice classes is already embedded, and the ETOPO5 [*National Geophysical Data Center*, 1988] digital elevation model is used for topography.

The RAP pattern for 13 March 2008 is consistent with the VC BrO distribution on the same date including: the well-defined vortex pattern with its center to the east of Victoria Island, the split in the Beaufort Sea toward the west and into the North Slope (indicated by arrows in the upper left panel in Figures 4 and 5), and the encroachment of BrO into the Canadian Shield region. The slight eastern offset of the RAP vortex center relative to the VC BrO vortex center was likely caused by the inherent uncertainty in NCEP wind fields. On 14-15 March 2008, the RAP shows the intrusion of BrO deeper into the Canadian Shield region. By 15 March 2008, the RAP vortex pattern weakened, as indicated by its dilated center, which drifted to the east of Victoria Island. On 16 March 2008, the RAP moves westward, explaining the westward extension of VC BrO over the Beaufort Sea and the Alaskan North Slope. On 17-18 March 2008, the RAP vortex was still present around Victoria Island, while maintaining the intrusion into the Canadian Shield region corresponding to the persistence of high VC BrO in this region.

Constrained by the ETOPO5 DEM, the RAP trajectories were terminated by the Alaskan Brooks Range and the Canadian Richardson and Mackenzie Mountains. NCEP data indicated that RAP could generally reach up to 0.4 km in the first day and up to 0.7 km after 2-3 days. Most trajectories were limited to low altitudes with a height distribution of 82% of the

trajectories below 100 m, 9% between 100-300 m, 6% between 300-500 m, and only 3% at higher altitudes. This height distribution of the trajectories is consistent with the boundary layer height of about 500 m. We note that ozone DIAL data obtained at the CCGS Amundsen [*Seabrook et al*., 2011] showed that ozone depletions were mostly confined to about 200m above the surface between 13-15 March 2008. Such trajectories facilitate the transport of aerosols, with HOBr and HBr being recycled to photolabile bromine and BrO being formed in the catalytic removal of O_3. Because their elevations are much higher than the altitudes reached by the RAP, the Brooks Range and the Richardson and Mackenzie Mountains form a barrier between the Alaskan interior and the bromine explosion. In contrast, the Alaskan North Slope and the Canadian Shield region are exposed to the bromine. These results hold true not only for the dates presented in Figures 4 and 5, but also for all other days in spring 2008 from satellite observations. This provides evidence for a regional topographic control on the distribution of BrO.

A model approach has been proposed to account for the BrO portion descending from the stratosphere [*Salawitch et al*., 2010]. However, when Theys et al. [2011] used the model estimate, they found that "while some satellite observed plumes of enhanced BrO can be explained by stratospheric descending air, we show that most BrO hotspots are of tropospheric origin, although they are often associated to regions with low tropopause heights as well." This is consistent with the tropospheric origin of the BrO hot spot presented in this paper. In addition, Neuman et al. [2010] also showed that ozone depletion and active bromine enhancement were confined to the marine boundary layer that was capped by a temperature inversion at 200–500m altitude with aircraft measurements across the Beaufort and Chukchi Sea in April 2008. A different regional (Svalbard) study and at a different time (spring 2007), using aircraft data

[*Prados-Roman et al*., 2011], revealed that BrO in the boundary layer could be one order of magnitude larger compared to that in the free troposphere up to the tropopause.

The observed BrO pattern and the atmospheric pressure and wind pattern are correlated. If one would observe a correlation between VC BrO and atmospheric patterns only within a section or part of the atmospheric column, say around the tropopause and nowhere else in the whole vertical profile of the atmosphere, one might conclude that the BrO would be located around that section or that part of the atmosphere. However, the patterns of winds at different atmospheric temperatures or pressures are similar or coherent from the lower to the upper troposphere or even the lower stratosphere as shown in Figure 6. Thus, from the correlation between winds and VC BrO patterns, one may not be able to determine unambiguously the elevated BrO altitude in different sections of the troposphere or in the stratosphere. On the other hand, the topographic control observed in this study clearly places the VC BrO enhancement (or explosion) within the lowest troposphere in this region of the Arctic.

To avoid biases injected by uncertainty in a model approach to correct for the BrO portion descending from the stratosphere [*Salawitch et al*., 2010], the omega field [*Thompson*, 1961; *Clarke and Lawniczak*, 1962], characterizing whether air masses are descending or ascending through different altitudes connecting different levels in the troposphere and stratosphere, should be applied first to determine whether the model of BrO descending from the stratosphere is applicable or not. In our case, the air mass was ascending from the surface through the 200-mb level (12.9 km) at the area of the BrO hot spot (Figure 6), and not descending from the stratosphere. Thus, using a model for BrO descending from the stratosphere [*Salawitch et al*., 2010] is not applicable for the elevated BrO events reported in this study.

7. Comparison between Spring 2008 and Spring 2009

Since perennial sea ice loss was drastic in 2007, leading to the record low of summer sea ice extent, a comparison is first made to provide a perspective for the significance of perennial sea ice change in 2008 and 2009, which are the two years relevant to the IPY/CFL/OASIS focus of this paper. A significant reduction in perennial ice extent of 1.2×10^6 km^2 was observed by QS during the 2007-2008 freezing season between 1 October 2007 and 1 May 2008. The perennial ice extent was 0.5×10^6 km^2 larger on 1 October 2008 compared to that at the same time in 2007 as a result of the survival of more sea ice after the 2008 melt season. Nevertheless, during the 2008-2009 freezing season between 1 October 2008 and 1 May 2009, the reduction of perennial sea ice extent was 50% more rapid than that during the same period in 2007-2008. The extent of Arctic perennial sea ice remained low in spring 2009. Perennial ice extent on 1 May 2009 was 2.1×10^6 km^2, which given the QS uncertainty of $\pm0.2\times10^6$ km^2, essentially equalled 2.2×10^6 km^2 of perennial ice extent observed on 1 May 2008. Although the extent of perennial ice was similar, its distribution differed between the two years. As shown by the red areas in Figure 7, there was a significant perennial ice reduction in BSAG in March 2009. Also, over most of BSAG, the surface air temperature (SAT) was lower in March 2009 compared to that in March 2008. In March 2009, the temperature decrease shown by the continuous contour lines in Figure 7, was more pronounced in the Canadian Arctic archipelago sector, compared to that in the Beaufort Sea sector.

In spring 2009, given the larger extent of saltier seasonal ice, together with the colder conditions in BSAG, stronger bromine explosions could be expected and were observed in VC BrO retrieved from the GOME-2 satellite data. Figure 8 shows the difference in VC BrO (Δ VC BrO) between those values averaged from March-May 2009 and those averaged for the same

period in 2008. The uncertainty in Δ VC BrO is estimated at 20% for ensemble averages consisting of independent samples of VC BrO measurement over a period of three months from March to May in 2008 and in 2009. The largest difference occurred in the region around the CFL field site (south of Banks Island and west of Victoria Island). Significant increases also occurred in the Beaufort Sea region to the west of Banks Island. Again and similar to spring 2008, the VC BrO distributions were limited to the north of Brooks Range and to the east of the Richardson and Mackenzie Mountains while no significant BrO was detected in the Alaskan interior.

The result presented above suggests an important hypothesis regarding potential impacts of Arctic sea ice reduction: If perennial sea ice continues to diminish and extreme temperature fluctuations increase cold spell occurrences, the abundance of saltier seasonal ice, polynyas, leads, and frost flowers may lead to more prevalent episodic events of bromine explosion and likely more severe tropospheric ozone and mercury depletion. This contrasts with another hypothesis proposing that an increasing trend in Arctic temperature may counteract effects from more extensive saltier seasonal ice associated with further perennial ice reduction in a warming climate, and thereby impede the efficiency of the bromine explosion effect [*Law and Stohl*, 2007; *Bottenheim et al*., 2009]. These two hypotheses are not necessarily contradictory because any change, including climate change, can be described by two different terms: a mean part representing an average trend, and a fluctuating part characterizing extreme conditions. The latter term predicting increasing extent of the conditions yielding bromine explosions is based on the more frequent cold periods, whereas the former term of impeding bromine explosions is based on an overall warming trend without taking into account strong temperature fluctuations.

8. Summary and Future Perspectives

This paper presents measurements of the recent decrease in Arctic perennial ice together with CFL/OASIS field measurements of trace atmospheric constituents and the tropospheric vertical columns of BrO retrieved from nadir measurements of backscattered radiation during the polar sunrise period in 2008 and 2009. Several key conclusions follow:

1. A drastic reduction of Arctic springtime perennial sea ice extent occurred in 2008 across the Arctic Ocean and it was further reduced in BSAG in 2009. In March, the low perennial ice extent in 2008 and 2009 shattered the 2007 record low by about one million km^2 while the total ice extent was similar in each year. This ice is replaced by a large expanse of younger and saltier seasonal ice, which is also more mobile and susceptible to divergence, during the time of polar sunrise, when the mechanisms of bromine explosions are active.
2. The timing of bromine oxide enhancement, under cold conditions, with the associated O_3 and GEM depletions observed by CFL/OASIS-CANADA ground-based field measurements and SCIAMACHY/GOME-2 satellite observations are consistent and explicable.
3. In 2008, a pronounced and well-defined vortex spiral pattern of the VC BrO, centered near the northeast coast of Victoria Island, and its evolution were observed by the GOME-2 satellite.
4. A RAP model describing the full three-dimensional characteristics of the atmospheric dynamics and their temporal evolution has been developed as opposed to using back trajectories as in past approaches. The RAP model shows the spatial conformity between the VC BrO vortex and the atmospheric spiral pattern in 2008.
5. Topography is found to constrain the distributions of BrO to the north of the Alaskan Brooks Range, and over the Canadian Shield region to the east of the Richardson and Mackenzie

Mountains, while in agreement with RAP patterns, the Alaskan interior was isolated from the bromine intrusion. This is consistent with the VC BrO being contained within the low troposphere for the cases observed in the BSAG region.

6. Stronger bromine explosions occurred in 2009, when perennial sea ice was reduced with the associated expansion of the saltier seasonal ice under colder conditions compared to those in 2008. Bromine explosions may be increased, if perennial sea ice continues to diminish and extreme temperature fluctuations increase cold spell occurrences.

Future study is required to fully understand the links between bromine sources and transport processes and the drastic Arctic sea ice decrease observed in the decade of the 2000s. The details of the role of polynyas, leads, and frost flowers in bromine source initiation are as yet speculative. Buoyant convective processes affecting plume formation and dynamics have not yet been incorporated into atmospheric chemistry models. Blowing snow may uplift sea salt aerosols to enhance bromine across snow-covered sea ice in the Antarctic, but drifting snow could also shut down bromine release when fresh snow buries saltier ice types in Arctic conditions. An analysis using decadal satellite datasets is necessary to determine whether the topography control on bromine distribution consistently holds true or may break down in some cases.

To further the understanding of the impacts of the reduction of sea ice on atmospheric photochemical processes and the oxidizing capacity of the lower atmosphere, the NASA BRomine, Ozone, and Mercury EXperiment (BROMEX) is planned for spring 2012 as an interdisciplinary research project [*Nghiem et al*., 2010]. While the topographic control on BrO distribution is reported in this paper, still to be investigated are the mechanisms of such control (simply by blocking, or by turbulent mixing, or rapid dilution in air forcing up by mountains,

etc.) and whether there is a difference in the amount of mercury deposition or tropospheric ozone between the Alaskan interior and the North Slope or the Canadian Shield region.

Regarding satellite data, past, present and future satellite missions are important and needed to provide long-term consistent datasets to help resolve our present science issues associated with bromine generation and fate and improve geophysical and chemical models. These are required to provide accurate projections of both Arctic changes and their impacts in a changing global environment and climate.

Acknowledgments.

The research carried out at the Jet Propulsion Laboratory, California Institute of Technology, and the Goddard Space Flight Center was supported by the National Aeronautics and Space Administration (NASA) Cryospheric Sciences Program. Rigor is funded by NOAA, NASA, NSF, and ONR. The research carried out by the University of Bremen team was supported in part by the German Aerospace, the European Union, and the State of Bremen. The views, opinions, and findings contained in this report are those of the authors and should not be construed as an official National Oceanic and Atmospheric Administration, or any other U.S. government position, policy, or decision. The CFL system study was funded by the Canadian Federal Program Office for the IPY and by the Natural Sciences and Engineering Research Council. The University of Manitoba was the lead agency in the international multiagency CFL project. The OASIS-Canada program was funded by the Canadian Federal Program Office for the IPY and by Environment Canada. Thanks to Alex Hare of the University of Manitoba for the photograph of frost flowers in Figure 2.

References

Abbatt, J., N. Oldridge, A. Symington, V. Chukalovskiy, R.D . McWhinney, S. Sjostedt, and R.A. Cox (2010), Release of gas-phase halogens by photolytic generation of OH in frozen halide-nitrate solutions: An active halogen formation mechanism?, *J. Phys. Chem., A, 114,* 6527–6533.

Alam, A., and J. Curry (1995), Lead-induced atmospheric circulation, *J. Geophys. Res.*, *100*(C3), 4643-4651.

Allen, W. L., ed. (1995), *National Geographic Atlas of the World*, Nat. Geogr. Soc., Washington D.C.

Allison, I. N. L. Bindoff, R. A. Bindschadler, P. M. Cox, N. de Noblet, M. H. England, J. E. Francis, N. Gruber, A. M. Haywood, D. J. Karoly, G. Kaser, C. Le Quéré, T. M. Lenton, M. E. Mann, B. I. McNeil, A. J. Pitman, S. Rahmstorf, E. Rignot, H. J. Schellnhuber, S. H. Schneider, S. C. Sherwood, R. C. J. Somerville, K. Steffen, E. J. Steig, M. Visbeck, A. J. Weaver (2009), *The Copenhagen Diagnosis*, *2009: Updating the World on the Latest Climate Science,* The University of New South Wales Climate Change Research Centre (CCRC), Sydney, Australia, 60pp.

AMAP/UNEP (2008), *Technical Background Report to the Global Atmospheric Mercury Assessment*, Arctic Monitoring and Assessment Programme / UNEP Chemicals Branch, 159 pp.

Barber, D. G, S. P. Reddan, and E. F. LeDrew (1995), Statistical characterization of the geophysical and electrical properties of snow on landfast first-year sea ice, *J. Geophys. Res*., *100*(C2), 2673-2686.

Barber, D. G., and S. V. Nghiem (1999), The role of snow on the thermal dependence of microwave backscatter over sea ice, *J. Geophys. Res.*, *104*(C11), 25789-25803.

Barber, D. G., M. Asplin, Y. Gratton, J. Lukovich, R. Galley, R. Raddatz, and D. Leitch (2010), The International Polar Year (IPY) Circumpolar Flaw Lead (CFL) System Study: Introduction and physical system, *Atmos.-Ocean, 48*(4), 225–243, doi:10.3137/OC317.2010.

Barrie, L. A., J. W. Bottenheim, R. C. Schnell, P. J. Crutzen, and R. A. Rasmussen (1988), Ozone destruction and photo-chemical reactions at polar sunrise in the lower Arctic atmosphere, *Nature*, *334*, 138-141.

Begoin, M., A. Richter, M. Weber, L. Kaleschke, X. Tian-Kunze, A. Stohl, N. Theys, and J. P. Burrows (2010), Satellite observations of long range transport of a large BrO plume in the Arctic, *Atmos. Chem. Phys*., 10, 6515-6526, doi:10.5194/acp-10-6515-2010.

Bottenheim, J. W., S. Netcheva, S. Morin, and S. V. Nghiem (2009), Ozone in the boundary layer air over the Arctic Ocean: Measurements during the TARA expedition, *Atmos. Chem. Phys.*, *9*, 4545-4557.

Burk, S. D., R. W. Fett, and R. E. Englebretson (1997), Numerical simulation of cloud plumes emanating from Arctic leads, *J. Geophys. Res.*, *102*(D14), 16529-16544.

Chaulk, A., G. A. Stern, D. Armstrong, D. Barber, and F. Wang (2011), Mercury distribution and transport across the ocean-sea ice-atmosphere interface in the Arctic Ocean. *Environ. Sci. Technol., 45*, 1866-1872.

Clark, L. C., and G. E. Lawniczak (1962), *Hemispheric Solution of the Omega Equation Including Terrain and Surface Frictional Effects*, Defense Technical Information Center, Naval Postgraduate School, Monterey, California, 162 pp.

Cole, A. S., and A. Steffen (2010), Trends in long-term gaseous mercury observations in the Arctic and effects of temperature and other atmospheric conditions, *Atmos. Chem. Phys.*, *10*, 4661-4672.

DAMOCLES (2009), TARA ARCTIC 2007-2009: The Great Arctic drift, http://www.damocles-eu.org/research/TARA_ARCTIC_2007-2008_The_Great_Arctic_drift_54.shtml, accessed 6 August 2009.

Dieckmann, G. S., G. Nehrke, C. Uhlig, J. Göttlicher, S. Gerland, M. A. Granskog, and D. N. Thomas (2010), Ikaite (CaCO3.6H2O) discovered in Arctic sea ice, *The Cryosphere*, *4*, 227-230., doi:10.5194/tc-4-227-2010.

DLR (2009), *Algorithm Theoretical Basis Document for GOME-2 Total Column Products of Ozone, Minor Trace Gases, and Cloud Properties*, Doc. No. DLR/GOME-2/ATBD/01, 36 pp., Oberpfaffenhofen, Germany.

DLR (2011), *SCIAMACHY Offline Processor Level1b-2 Algorithm Theoretical Baseline Document*, Doc. No. ENV-ATB-QWG-SCIA-0085, 137 pp., Oberpfaffenhofen, Germany.

Douglas, T., M. Sturm, W. R. Simpson, S. Brooks, S. E. Lindberg, and D. K. Perovich (2005), Elevated mercury measured in snow and frost flowers near Arctic sea ice leads, *Geophys. Res. Lett*., 32, L04502, doi:10.1029/2004GL022132.

Durnford, D., et al. (2011), Relationships between observations of cryospheric mercury and model environmental variables, *Journal of Geophysical Research*, submitted.

Fan, S.-M., and D. J. Jacob (1992), Surface ozone depletion in Arctic spring sustained by bromine reactions on aerosols, *Nature*, 359, 522-524.

Fishman, J. (1991), The global consequences of increasing tropospheric ozone concentrations, *Chemosphere*, *22*(7), 685-695.

Foster, K. L., R. A. Plastridge, J. W. Bottenheim, P. B. Shepson, B. J. Finlayson-Pitt, and C. W. Spencer (2001), The Role of Br2 and BrCl in surface ozone destruction at polar sunrise. *Science*, *291*, 471-474.

Frieß, U., J. Hollwedel, G. König-Langlo, T. Wagner, and U. Platt (2004), Dynamics and chemistry of tropospheric bromine explosion events in the Antarctic coastal region, *J. Geophys. Res*., *109*, D06305, doi:10.1029/2003JD004133.

Gauchard, P.-A., K. Aspmo, C. Temme, A. Steffen, C. Ferrari, T. Berg, J. Strom, L. Kaleschke, A. Dommergue, E. Bahlmann, O. Magan,d, F. Planchon, R. Ebinghaus, C. Banic, S. Nagorski, P. Baussand, and C. Boutron (2005), Study of atmospheric mercury depletion events recorded in Ni-Ålesund, Svalbard, spring 2003, *Atmos. Envir*., *39*, 7620-7632.

Glendening, J. W. (1995), Horizontally integrated atmospheric heat flux from an Arctic lead, *J. Geophys. Res.*, *100*(C3), 4613-4620.

Hall, J. S., and E. W. Wolff, (1998), Causes of seasonal and daily variations in aerosol sea-salt concentrations at a coastal Antarctic station, *Atmos. Environ*., *32*, 3669– 3677.

Hall, D. K., J. R. Key, K. A. Casey, G. A. Riggs, and D. J. Cavalieri (2004), Sea ice surface temperature product from MODIS, *IEEE Trans. Geosci. Remote Sens., 42*, 1,076-1,087.

Huff, A. K., and J. P. D. Abbatt (2002), Kinetics and product yields in the heterogeneous reactions of HOBr with ice surfaces containing NaBr and NaCl, *J. Phys. Chem. A, 106,* 5279-5287.

Jacobi, H.-W., L. Kaleschke, A. Richter, A. Rozanov, and J. P. Burrows (2006), Observation of a fast ozone loss in the marginal ice zone of the Arctic Ocean, *J. Geophys. Res*., *111*, D15309, doi:10.1029/2005JD006715.

Jones, A. E., P. S. Anderson, E. W. Wolff, H. K. Roscoe, G. J. Marshall, A. Richter, N. Brough, and S. R. Colwell (2010), Vertical structure of Antarctic tropospheric ozone depletion events: characteristics and broader implications, *Atmos. Chem. Phys*., 10, 7775–7794, www.atmos-chem-phys.net/10/7775/2010/, doi:10.5194/acp-10-7775-2010.

Kaleschke, L., A. Richter, J. P. Burrows, O. Afe, G. Heygster, J. Notholt, A. M. Rankin, H. K. Roscoe, J. Hollwedel, T. Wagner, and H.-W. Jacobi (2004), Frost flowers on sea ice as a source of sea salt and their influence on tropospheric halogen chemistry, *Geophys. Res. Lett*., *31*, L16114, doi:10.1029/2004GL020655.

Kalnay, E., M. Kanamitsu, R. Kistler, W. Collins, D. Deaven, L. Gandin, M. Iredell, S. Saha, G. White, J. Woollen, Y. Zhu, A. Leetmaa, R. Reynolds, M. Chelliah, W. Ebisuzaki, W. Higgins, J. Janowiak, K. C. Mo, C. Ropelewski, J. Wang, R. Jenne, and D. Joseph (1996), The NCEP/NCAR 40-year reanalysis project, *Bull. Amer. Meteor. Soc. 77*, 437-471.

Lalonde, J. D., M. R. Doyon, and J. C. Auclair (2003), Photo-induced Hg(II) reduction in snow from the remote and temperate Experimental Lakes Area (Ontario, Canada), *J. Geophysical Res.*, *108*(D6), 4200, doi:10.1029/2001JD001534.

Law, K. S., and A. Stohl (2007), Arctic air pollution: Origins and impacts, *Science*, *315*, 1537-1540, doi:10.1126/science.1137695.

Lu, J. Y., W. H. Schroeder, L. A. Barrie, A Steffen, H. E. Welch, K. Martin, L. Lockhart, R. V. Hunt, G. Boila, and A. Richter (2001), Magnification of atmospheric mercury deposition to polar regions in springtime: the link to tropospheric ozone chemistry, *Geophys. Res. Lett., 28*(17), 3219-3222.

Martin, S., R. Ducker, and M. Fort (1995), A laboratory study of frost flower growth on the surface of young sea ice, *J. Geophys. Res*., *100*, 7027-7036.

Martin, S., Y. Yu, and R, Drucker (1996), The temperature dependence of frost flower growth on laboratory sea ice and the effect of the flowers on infrared observations of the surface, *J. Geophys. Res*., *101*, 12,111-12,125.

Maslanik, J. A., C. Fowler, J. Stroeve, S. Drobot, J. Zwally, D. Yi, and W. Emery (2007), A younger, thinner Arctic ice cover: Increase potential for rapid, extensive sea-ice loss, *Geophys. Res. Lett*., *34*(24), L24501, doi:10.1029/2007GL032043.

McElroy, C. T., C. A. McLinden, and J. C. McConnell (1999), Evidence for bromine monoxide in the free troposphere during Arctic polar sunrise, *Nature, 397***,** 338-340.

National Geophysical Data Center (1988), *Digital relief of the Surface of the Earth*, Data Announcement 88-MGG-02, NOAA, Boulder, Colorado.

Neuman, J. A., J. B. Nowak, L. G. Huey, J. B. Burkholder, J. E. Dibb, J. S. Holloway, J. Liao, J. Peisch, J. M. Roberts, T. B. Ryerson, E. Scheuer, H. Stark, R. E. Stickel, D. J. Tanner, and A. Weinheimer (2010), Bromine measurements in ozone depleted air over the Arctic Ocean, *Atmos. Chem. Phys*., *10*, 6503–6514.

Nghiem, S. V., R. Kwok, S. H. Yueh, and M. R. Drinkwater (1995), Polarimetric signature of sea ice – 2. Experimental observations, *J. Geophys. Res., 100*, 13681-13698.

Nghiem, S. V., S. Martin, D. K. Perovich, R. Kwok, R. Drucker, and A. J. Gow (1997a), A laboratory study of the effect of frost flowers on C band radar backscatter from sea ice, *J. Geophys. Res*., *102*, 3357-3370.

Nghiem, S. V., R. Kwok, S. H. Yueh, A. J. Gow, D. K. Perovich, J. A. Kong, and C. C. Hsu (1997b), Evolution in polarimetric signature of thin saline ice under constant growth, *Radio Sci., 32*, 127-151.

Nghiem, S. V., I. G. Rigor, D. K. Perovich, P. Clemente-Colón, J. W. Weatherly, and G. Neumann (2007), Rapid reduction of Arctic perennial sea ice, *Geophys. Res. Lett*., *34*, L19504, doi:10.1029/2007GL031138.

Nghiem, S. V., I. G. Rigor, P. Clemente-Colón, A. Freeman, A. Richter, J. P. Burrows, P. B. Shepson, J. Bottenheim, D. G. Barber, W. Simpson, D. K. Perovich, M. Sturm, A. Steffen, L. Kaleschke, D. K. Hall, T. Markus, H. Eicken, and G. Neumann (2010), Rejuvenation of Arctic sea ice and tropospheric chemical change, Abst. C43D-0580 presented at 2010 Fall Meeting, AGU, San Francisco, Calif., 13-17 Dec.

Outridge, P. M., R. W. Macdonald, F. Wang, G. A. Stern, and A. P. Dastoor (2008), A mass balance inventory of mercury in the Arctic Ocean, *Environ. Chem., 5*, 89-111.

Perovich, D. K., and J. A. Richter-Menge (1994), Surface characteristics of lead ice. *J. Geophys. Res*., *99*, 16341-16350.

Perovich, D. K., J. Richter-Menge, K. F. Jones, and B. Light (2008), Sunlight, water, and ice: Extreme Arctic sea ice melt during summer 2007, *Geophys. Res. Lett*., *35*(11), L11501, doi:10.1029/2008GL034007.

Pinto, J. O., J. A. Curry, and K. L. McInnes (1995), Atmospheric convective plumes emanating from leads. 1. Thermodynamic structure, *J. Geophys. Res.*, *100*(C3), 4621-4631.

Pinto, J. O., and J. A. Curry (1995), Atmospheric convective plumes emanating from leads. 2. Microphysical and radiative processes, *J. Geophys. Res.*, *100*(C3), 4633-4642.

Piot, M., and R. von Glasow (2008), The potential importance of frost flowers, recycling on snow, and open leads for ozone depletion events, *Atmos. Chem. Phys*., *8*, 2437-2467.

Pöhler, D., L. Vogel, U. Frieß, and U. Platt (2010), Observation of halogen species in the Amundsen Gulf, Arctic, by active long-path differential optical absorption spectroscopy, *Proc. Nat. Acad. Science*, 107, 6582-6587.

Prados-Roman, C., A. Butz, T. Deutschmann, M. Dorf, L. Kritten, A. Minikin, U. Platt, H. Schlager, H. Sihler, N. Theys, M. Van Roozendael, T. Wagner, and K. Pfeilsticker (2011), Airborne DOAS limb measurements of tropospheric trace gas profiles: case studies on the profile retrieval of O4 and BrO, *Atmos. Meas. Tech*., *4*, 1241–1260.

Rankin, A. M., E. W. Wolff, and S. Martin (2002), Frost flowers: Implications for tropospheric chemistry and ice core interpretation, *J. Geophys. Res*., *107*, 4683, doi:10.1029/2002JD002492.

Richter, A., F. Wittrock, M. Eisinger, and J. P. Burrow (1998), GOME observations of tropospheric BrO in northern hemispheric spring and summer 1997, *Geophys. Res. Lett*., *25*(14), 2683-2686.

Richter-Menge, J., J. Comiso, W. Meier, S. Nghiem, and D. Perovich (2008), Sea Ice Cover, in *State of the Climate in 2007*, *Bull. Amer. Meteorol. Soc*., *89*(7), S1-S179.

Ridley, B. A., T. Zeng, Y. Wang, E. L. Atlas, E. V. Browell, P. G. Hess, J. J. Orlando, K. Chance, and A. Richter (2007), An ozone depletion event in the sub-arctic surface layer over Hudson Bay, Canada, *J. Atmos. Chem*., *57*, 255-280.

Rigor, I. G., R. L. Colony, and S. Martin (2000), Variations in surface air temperature observations in the Arctic, 1979-97, *J. Clim*., *13*, 896-914.

Rysgaard, D., R. N. Glud, K. Lennert, M. Cooper, N. Halden, R. J. G. Leaky, and D. Barber (2011), Ikaite crystals in melting sea ice leads to low *p*CO2 levels and high pH in Arctic surface waters, *J. Geophys. Res*., in review.

Salawitch, R.J., T. Canty, T. Kurosu, K. Chance, Q. Liang, A. da Silva, S. Pawson, J. E. Nielsen, J. M. Rodriguez, P. K. Bhartia, X. Liu, L. G. Huey, J. Liao, R. E. Stickel, D. J. Tanner, J. E. Dibb, W. R. Simpson, D. Donohoue, A. Weinheimer, F. Flocke, D. Knapp, D. Montzka, J. A. Neuman, J. B. Nowak, T. B. Ryerson, S. Oltmans, D. R. Blake, E. L. Atlas, D. E. Kinnison, S. Tilmes, L. L. Pan, F. Hendrick, M. Van Roozendael, K. Kreher, P. V. Johnston, R. S. Gao, B. Johnson, T. P. Bui, G. Chen, R. B. Pierce, J. H. Crawford, and D. J. Jacob (2010), A new interpretation of total column BrO during Arctic spring, *Geophys. Res. Lett*., *37*, L21805, doi:10.1029/2010GL043798.

Sander, R., J. Burrows, and L. Kaleschke (2006), Carbonate precipitation in brine – A potential trigger for tropospheric ozone depletion events, *Atm. Chem. Phys., 6*, 4653-4658.

Sander, R., and S. Morin (2009), Introducing the bromide/alkalinity ratio for a follow-up discussion on "Precipitation of salts in freezing seawater and ozone depletion events: a status

report", by Morin et al., published in *Atmos. Chem. Phys*., *8*, 7317–7324, 2008, *Atmos. Chem. Phys. Discuss*., *9*, 20765–20773, http://www.atmos-chem-phys-discuss.net/9/20765/2009/.

Schnell, R. C., R. G. Barry, M. W. Miles, E. L. Andreas, L. F. Radke, C. A. Brock, M. P. McCormick, and J. L. Moore (1989), Lidar detection of leads in Arctic sea ice, *Nature*, *339*, 530-532.

Schroeder, W. H., K. G. Anlauf, J. Y. Lu, A. Steffen, D. R. Schneeberger, and T. Berg (1998), Arctic springtime depletion of mercury, *Nature*, *394*, 331-332.

Seabrook, J. A., J. Whiteway, R. M. Stæbler, J. W. Bottenheim, L. Komguem, L. H. Gray, D.Barber, M. Asplin (2011), LIDAR measurements of Arctic Boundary Layer Ozone Depletion Events Over the Frozen Arctic Ocean, in press (it is part of this special issue).

Shepson, P., P. Matrai, L. Barrie, and J. Bottenheim (2003), Ocean-atmosphere-sea ice-snowpack interactions in the Arctic, and global change, *Eos, 84*, 349, 355.

Sherman, L. S., J. D. Blum, K. P. Johnson, G. J. Keeler, J. A. Barres, and T. A. Douglas (2010), Mass-independent fractionation of mercury isotopes in Arctic snow driven by sunlight, *Nature Geosci.*, *3*(3), 173-177.

Simpson, W. R., D. Carlson, G. Hönninger, T. A. Douglas, M. Sturm, D. Perovich, and U. Platt (2007), First-year sea-ice contact predicts bromine monoxide (BrO) levels at Barrow, Alaska better than potential frost flower contact, *Atmos. Chem. Phys*., *7*, 621-627.

Simpson, W. R., R. von Glasow, K. Riedel, P. Anderson, P. Ariya, J. Bottenheim, J. Burrows, L. J. Carpenter, U. Frieß, M. E. Goodsite, D. Heard, M. Hutterli, H.-W. Jacobi, L. Kaleschke, B. Neff, J. Plane, U. Platt, A. Richter, H. Roscoe, R. Sander, P. Shepson, J. Sodeau, A. Steffen,

T. Wagner, and E.Wolff (2007), Halogens and their role in polar boundary-layer ozone depletion. *Atmos. Chem. Phys*., *7*, 4375-4418.

St. Louis, V. L., M. J. Sharp, A. Steffen, A. May, J. Barker, J. L. Kirk, D. J. A. Kelly, S. E. Arnott, B. Keatley, and J. P. Smol (2005), Some sources and sinks of monomethyl and inorganic mercury on Ellesmere Island in the Canadian high arctic, *Environ. Sci. Tech.*, *39*(8), 2686-2701.

Steffen, A., W. Schroeder, R. MacDonald, L. Poissant, and A. Konoplev (2005), Mercury in the Arctic atmosphere: An analysis of eight years of measurements of GEM at Alert (Canada) and a comparison with observations at Amderma (Russia) and Kuujjuarapik (Canada), *Sci. Total Environ., 342*, 185-198.

Steffen, A., T. Douglas, M. Amyot, P. Ariya, K. Aspmo, T. Berg, J. Bottenheim, S. Brooks, F. Cobbett, A. Dastoor, A. Dommergue, R. Ebinghaus, C. Ferrari, K. Gardfeldt, M. E. Goodsite, D. Lean, A. Poulain, C. Scherz, H. Skov, J. Sommar, and C. Temme (2008), A synthesis of atmospheric mercury depletion event chemistry in the atmosphere and snow, *Atmos. Chem. Phys*., *8*(6), 1445-1482.

Stephens, C. R., P. B. Shepson, A. Steffen, J. W. Bottenheim, J. Liao, L. G. Huey, E. Apel, A. Weinheimer, S. V. Nghiem, and S. R. Hall (2011), Observations of the relative importance of chlorine and bromine radicals in the oxidation of elemental mercury at Barrow, AK, *J. Geophys. Res.,* submitted.

Stroeve, J., M. M. Holland, W. Meier, T. Scambos, and M. Serreze (2007), Arctic sea ice decline: Faster than forecast, *Geophys. Res. Lett*., *34*, L09501, doi:10.1029/2007/GL029703.

Sinnhuber, B.-M., A. Rozanov, N. Sheode, O. T. Afe, M. Sinnhuber, F. Wittrock, J. P. Burrow, G. P. Stiller, T. von Clarmann, and A. Linden (2005), Global observations of stratospheric bromine from SCIAMACHY, *Geophys. Res. Lett*., *32*, L20810, doi:10.1029/2005GL023839.

Sturges, W. T., G. F. Cota, and P. T. Buckley (1997), Vertical profile of bromoform in snow, sea ice, and seawater in the Canadian Arctic, *J. Geophys. Res*., *102*(C11), 25073-25083.

Tarasick, D. W., and J. W. Bottenheim (2002), Surface ozone depletion episodes in the Arctic and Antarctic from historical ozonesonde records, *Atmos. Chem. Phys., 2*, 197-205.

Theys, N., M. Van Roozendae, Q. Errera, F. Hendrick, F. Daerden1, S. Chabrillat, M. Dorf, K. Pfeilsticker, A. Rozanov, W. Lotz, J. P. Burrows, J.-C. Lambert, F. Goutail, H. K. Roscoe, and M. De Mazière (2009), A global stratospheric bromine monoxide climatology based on the BASCOE chemical transport model, *Atmos. Chem. Phys*., *9*, 831–848.

Theys, N., M. Van Roozendael, F. Hendrick, X. Yang, I. De Smedt, A. Richter, M. Begoin, Q. Errera, P. V. Johnston, K. Kreher, and M. De Mazière (2011), Global observations of tropospheric BrO columns using GOME-2 satellite data, Atmos. Chem. Phys., *11*, 1791–1811, 2011.

Thompson, P. D. (1961), *Numerical Weather Analysis and Prediction,* The MacMillan Co., New York, 170 pp.

UNEP (2011), *Report of the intergovernmental negotiating committee to prepare a global legally binding instrument on mercury on the work of its second session*, United Nations Environment Programme, UNEP (DTIE)/Hg/INC.2/20.

Wakatsuchi, M., and N. Ono (1983), Measurements of salinity and volume of brine excluded from growing sea ice, *J. Geophys. Res*., *88*, 2943-2951.

Weeks, W. F., and S. F. Ackley (1982), The growth, structure, and properties of sea ice, *CRREL Monograph 82-1*, U.S. Army Cold Regions Res. Eng. Lab., Hanover, N.H.

Wennberg, P. (1999), Atmospheric chemistry – Bromine explosion, *Nature*, *397*, 299-301.

Zulauf, M. A., and S. Krueger (2003), Two-dimensional numerical simulations of Arctic leads: Plume penetration height, *J. Geophys. Res*., *108*(C2), 8050, doi:10.1029/2000JC000495.

Figure 1. Chart of different interdisciplinary IPY research components contributing to the focus effort to understand Arctic photochemical source, process, transport, and distribution.

Figure 2. Arctic sea ice conditions during the study. Panel (a) presents the synoptic state of Arctic sea ice on 15 March 2008. The QS sea ice map consists of perennial sea ice (white), seasonal sea ice (aqua), mixed ice (cyan), ocean (blue), land (brown), and missing data at the North Pole (black). The QS map is translucently overlaid on a grey-tone Envisat SAR image so that perennial ice (P) appears grey, seasonal ice (S) appears dark aqua, and mixed ice (M) appears green. V and B respectively represent Victoria and Banks Islands, O is for ocean, and the large circle around the North Pole is the area of missing Envisat data. The inset is a MODIS image of ice surface temperature averaged over the period of 12-19 March 2008. In the MODIS image inset, B stands for Banks Island and the magenta areas represent cloud cover (mostly in the north east of B). Panel (b) is a high-resolution RADARSAT SAR image, acquired on 16 March 2008 around the CFL field experimental area in the Amundsen Gulf located at the white square on panel (a). The ellipse marks an example of a lead, appeared as a bright elongated feature (all other bright leads are not marked). In panel (b), the southern tip of Banks Island is seen at the lower right corner. Panel (c) is a photograph of frost flowers taken on 16 March 2008 at the Amundsen field location near the tip of the arrow in panel (b).

Figure 3. Variations of temperatures, BrO, O_3, and GEM in March 2008. The black upward arrows mark the timing of BrO increase and O_3 and GEM depletion episodes. The orange double-arrow lines bracket the time period (12-19 March 2008) when GOME-2 and SCIAMACHY detected the BrO enhancement. The magenta downward arrows indicate the

timing of blowing snow events observed in the Amundsen Gulf. There error bars are: ±0.5°C for buoy air temperature, ±1.3°C for MODIS ice surface temperature, ±30% for VC BrO, ±15% for OASIS BrO, ±1 ppb for OASIS O_3, and ±10% for CFL GEM.

Figure 4. Total BrO in the vertical column (VC) measured by the GOME-2 scanning spectrometer on days 73-78 (13-18 March) in 2008.

Figure 5. Trajectory patterns of air parcels rising from seasonal and mixed sea ice estimated from NCEP three-dimensional wind vectors on days 73-78 (13-18 March) in 2008. The color scale (orange-red) represents the height of trajectories of rising air originating within the sector from the Arctic Circle to 78°N and longitudes between 80°W to 160°W, which includes the Beaufort Sea and the western Canadian Arctic Archipelago. Yellow denotes trajectories of air parcels rising from seasonal and mixed ice outside this sector. Vectors indicate speeds and directions of horizontal wind components.

Figure 6. Atmospheric patterns at different levels in the troposphere and the stratosphere on 13 May 2008. Vectors represent horizontal wind speed and direction, green contours for positive vertical wind in cm/s (i.e., rising air), grey contours for the iso-lines of 0 cm/s in vertical wind, and blue contours for surface level pressure (top left panel).

Figure 7. Difference in sea ice classes between 15 March in 2008 and 2009. Perennial sea ice (PI) is distinguished from other sea ice classes (OT) including seasonal ice and mixed ice, and from open water (OW). White represents areas where there was PI in both 2008 and 2009, blue

for PI in 2009 and OT in 2008, red for OT in 2009 and PI in 2008 (i.e., loss of perennial ice in 2009 compared to 2008), darker blue for OT in both 2008 and 2009, darkest blue for OW in 2008 or 2009, and grey for land. Continuous (dotted) green contour lines represent surface air temperature decrease (increase) in 2009 compare to that in 2008.

Figure 8. Difference in GOME-2 VC BrO averaged over the period of March-May as defined by Δ VC BrO (March-May) = VC BrO (March-May 2009) – VC BrO (March-May 2008). Uncertainty in Δ VC BrO is estimated at 20% for ensemble averages consisting of independent samples of VC BrO measurement over a period of three months from March to May in 2008 and in 2009.

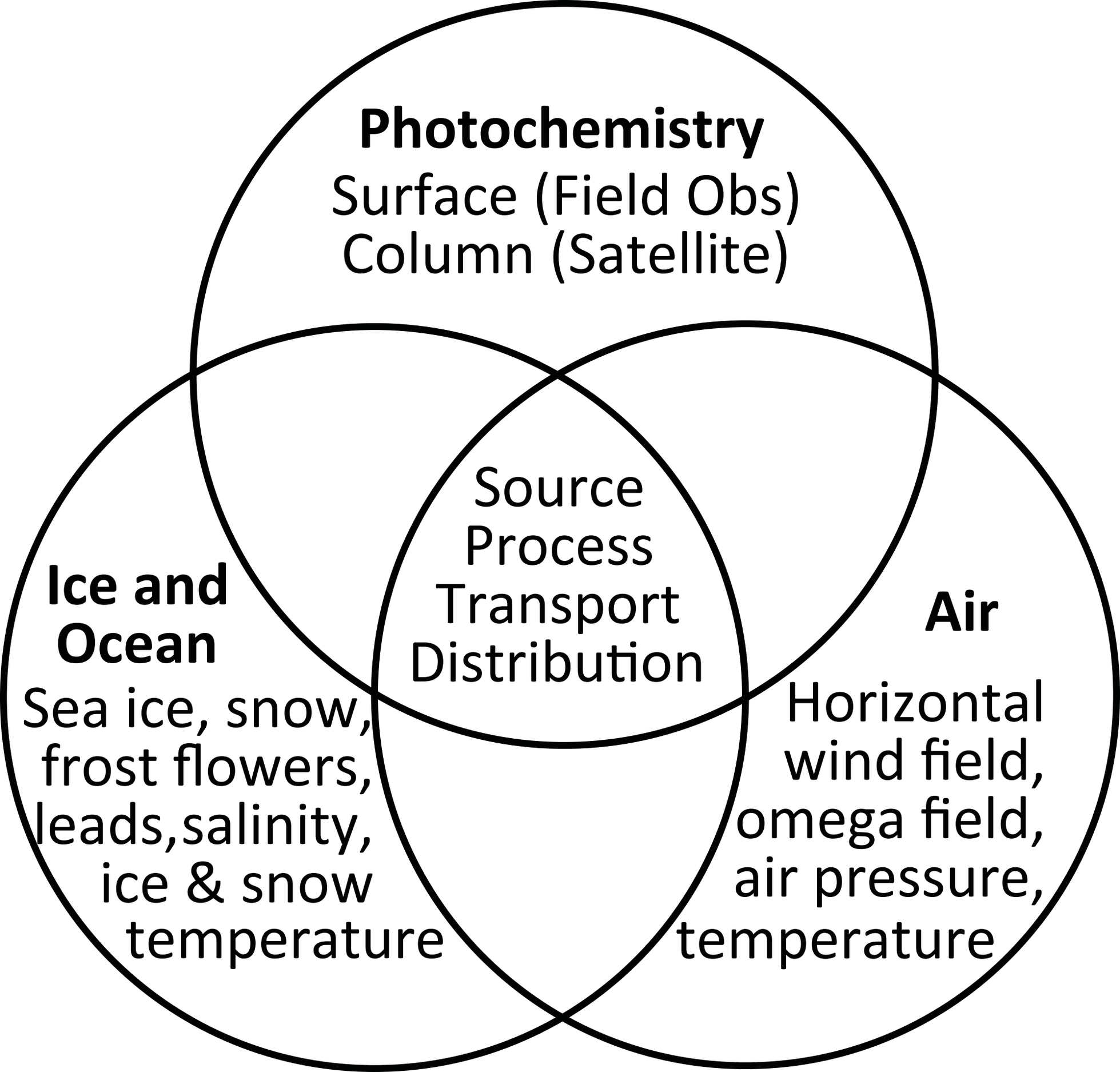
Photochemistry
Surface (Field Obs)
Column (Satellite)
Source
Process
Transport
Distribution
Ice and Ocean
Sea ice, snow, frost flowers, leads,salinity, ice & snow temperature
Air
Horizontal wind field, omega field, air pressure, temperature

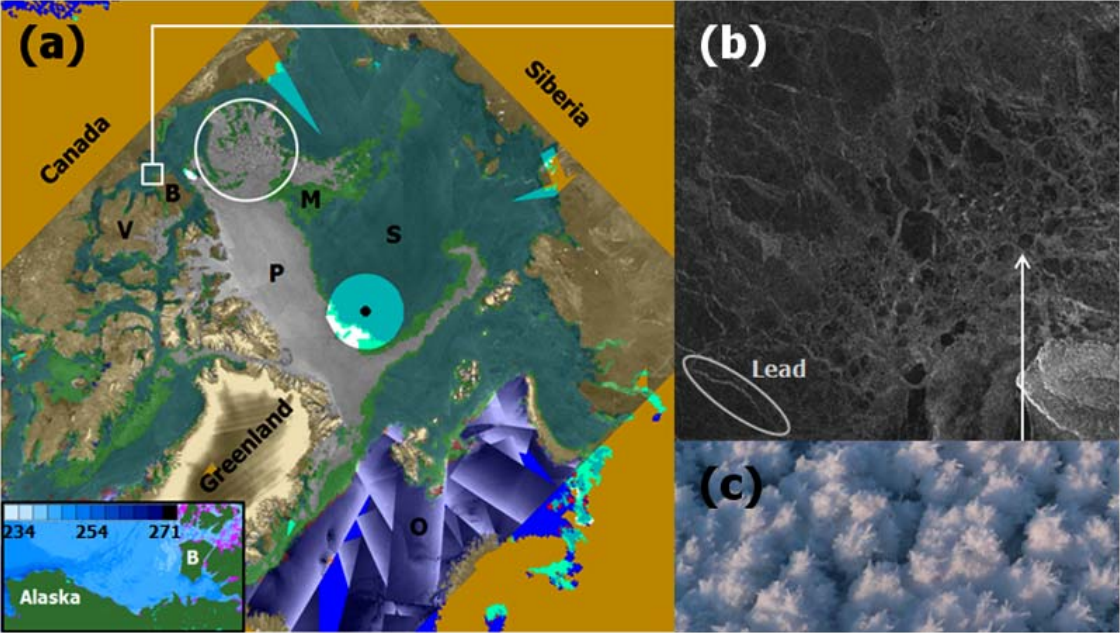
(a)
Canada
Siberia
B
V
M
S
P
Greenland
O
234
254
271
B
Alaska
(b)
Lead
(c)

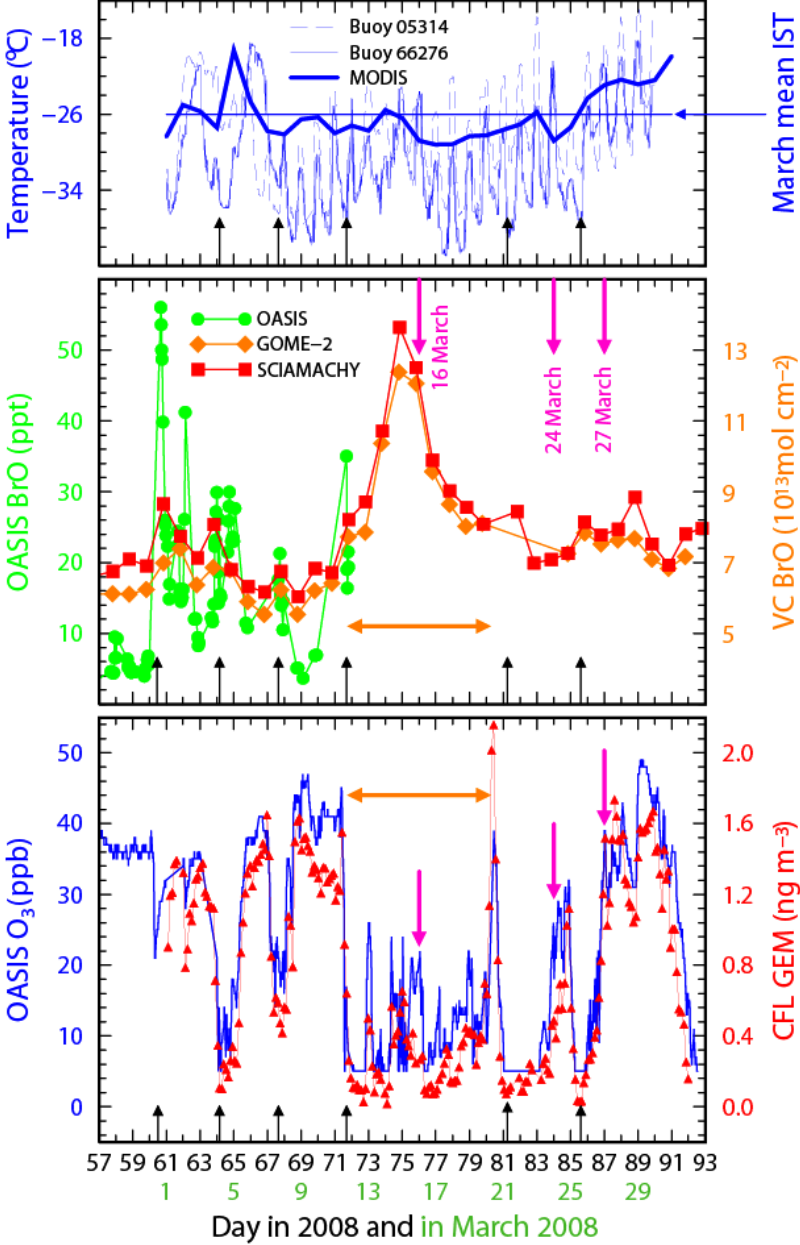
Temperature (°C)
−18
−26
−34
Buoy 05314
Buoy 66276
MODIS
March mean IST
OASIS BrO (ppt)
50
40
30
20
10
OASIS
GOME−2
SCIAMACHY
16 March
24 March
27 March
VC BrO (10¹³mol cm⁻²)
13
11
9
7
5
OASIS O₃(ppb)
50
40
30
20
10
0
CFL GEM (ng m⁻³)
2.0
1.6
1.2
0.8
0.4
0.0
57 59 61 63 65 67 69 71 73 75 77 79 81 83 85 87 89 91 93
1 5 9 13 17 21 25 29
Day in 2008 and in March 2008

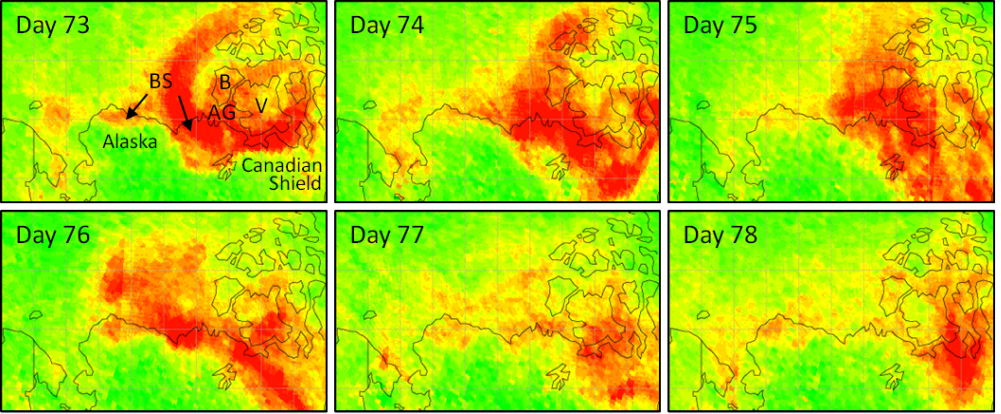
Day 73
BS
B
AG
V
Alaska
Canadian Shield
Day 74
Day 75
Day 76
Day 77
Day 78
VC BrO
[mol cm⁻²]
>
9.0 10¹³
8.0 10¹³
7.0 10¹³
6.0 10¹³
5.0 10¹³
4.0 10¹³
<

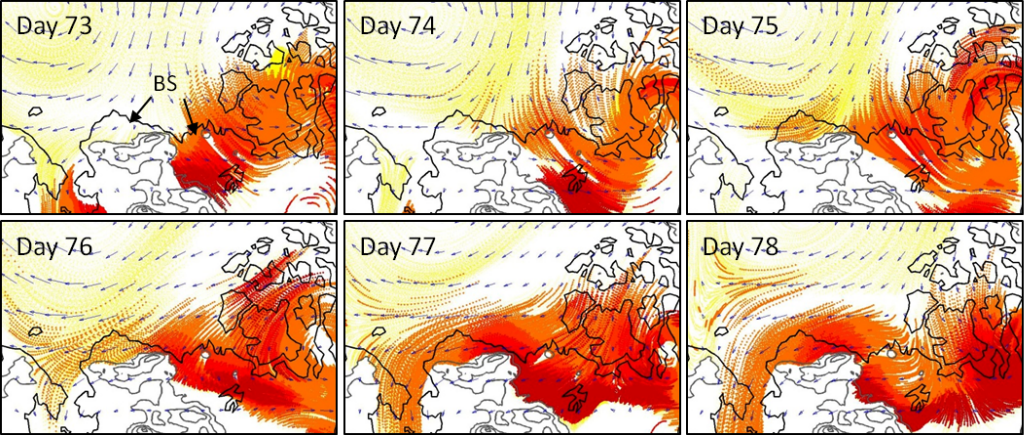
Day 73
BS
Day 74
Day 75
Day 76
Day 77
Day 78
Height
[meter]
>
500
400
300
200
100
0
10 m/s

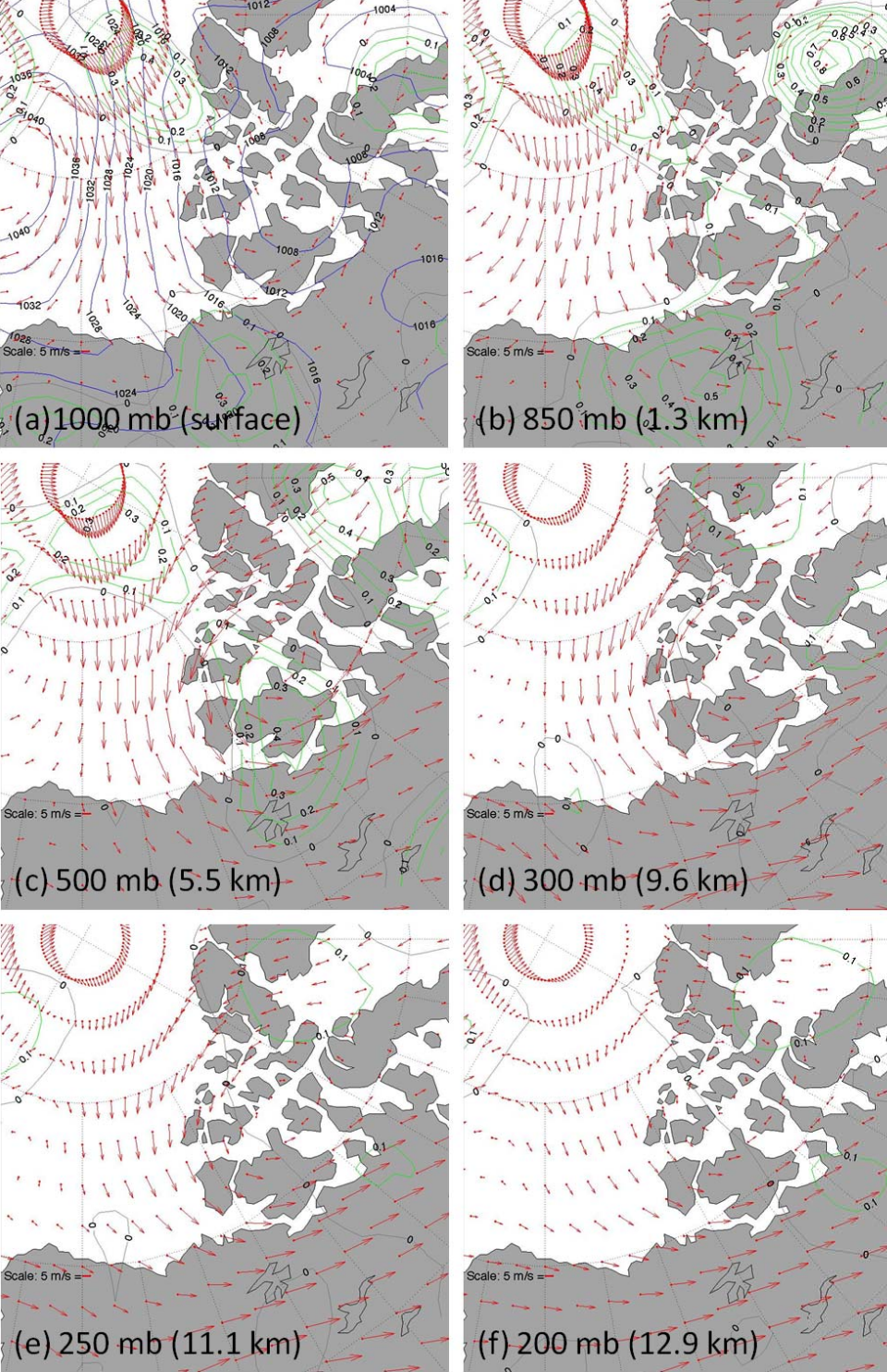
(a) 1000 mb (surface)
(b) 850 mb (1.3 km)
(c) 500 mb (5.5 km)
(d) 300 mb (9.6 km)
(e) 250 mb (11.1 km)
(f) 200 mb (12.9 km)
Scale: 5 m/s

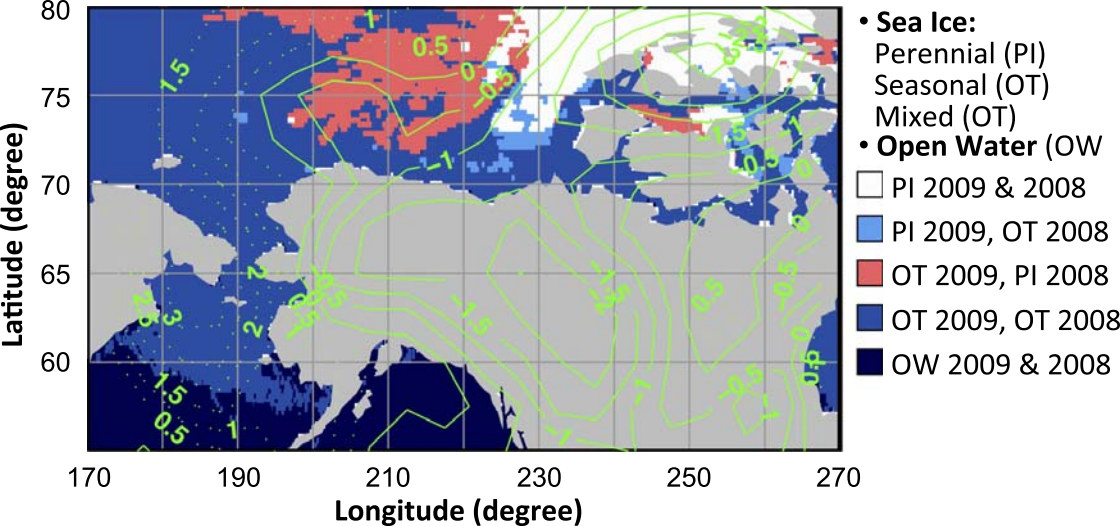
80
75
70
65
60
Latitude (degree)
170
190
210
230
250
270
Longitude (degree)
• Sea Ice:
Perennial (PI)
Seasonal (OT)
Mixed (OT)
• Open Water (OW
PI 2009 & 2008
PI 2009, OT 2008
OT 2009, PI 2008
OT 2009, OT 2008
OW 2009 & 2008

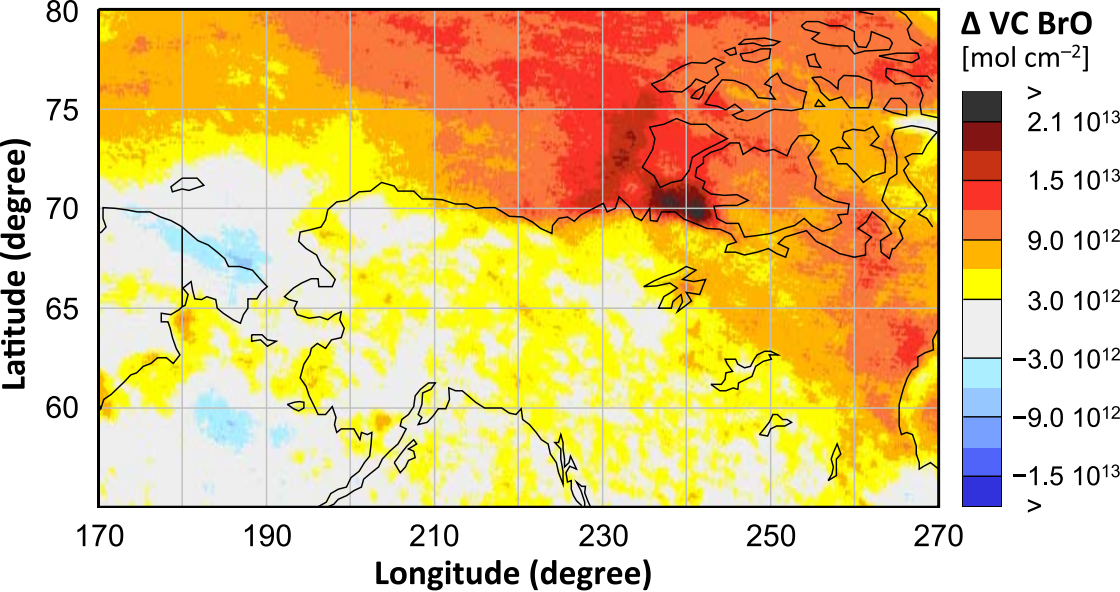
Δ VC BrO
[mol cm⁻²]
>
2.1 10¹³
1.5 10¹³
9.0 10¹²
3.0 10¹²
−3.0 10¹²
−9.0 10¹²
−1.5 10¹³
>
Latitude (degree)
80
75
70
65
60
170
190
210
230
250
270
Longitude (degree)

Figure 8